Towards an enhanced fatigue evaluation of bituminous mortars

Towards an enhanced fatigue evaluation of bituminous mortars

Article *in* Construction and Building Materials · November 2020

DOI: 10.1016/j.conbuildmat.2020.121578

Towards an enhanced fatigue evaluation of bituminous mortars

Alexandros Margaritis [a], Georgios Pipintakos [a], Aikaterini Varveri [b], Geert Jacobs [a], Navid Hasheminejad [a], Johan Blom [a], Wim Van den bergh [a]*

[a] University of Antwerp, Antwerp, Belgium

[b] Delft University of Technology, Delft, the Netherlands

**corresponding author: alexandros.margaritis@uantwerpen.be*

Abstract

The fatigue resistance, as a performance indicator, is of paramount importance for the selection and benchmarking of bituminous materials. The bituminous mortar can be considered as the medium that connects and envelopes the coarse aggregate skeleton, and hence will significantly influence the fatigue resistance at bulk-scale. Therefore this study presents the steps and challenges of a new testing framework to evaluate the fatigue resistance of bituminous mortars. To do so, first, a new test geometry is introduced, which will ensure cohesive failure in a predefined area. The integrity of this sample geometry is assessed theoretically through finite element simulations and by computer tomography scans. Secondly, specimens of the new geometry are evaluated experimentally using a dynamic shear rheometer, where time-sweep tests are performed on two control mortar types under various test conditions. The control mortar types are fabricated using two commercial bituminous binders, one modified and one neat binder, to evaluate the effect of binder type. The test results are comprehensively analysed using fundamental dissipated energy-based concepts but also empirical and phenomenological failure criteria, providing insights into the failure evolution. For the tested mortar types, the analysis shows good convergence with the considered fatigue models. Finally, using dissipated energy concepts led to the most consisted fatigue model, which is independent of binder type and test conditions.

Keywords: Bituminous mortar; Fatigue resistance; Dynamic shear rheometer; Dissipated energy ratio; Ratio of dissipated energy change;

1. Introduction

Nowadays, the majority of road infrastructure worldwide is composed of flexible pavements that consist of different asphaltic layers, where each layer fulfils certain functions. To ensure the service life of such pavement structures, it is essential to design the pavement and more specifically, its mixtures considering the expected traffic load it should withstand. Typical requirements are stiffness and resistance against fatigue and rutting. Since an asphalt mixture is a heterogeneous material, the composition and characteristics of the components greatly influence its performance. Asphalt mixtures typically consist of a mineral skeleton (stones, sand and filler) and a bituminous binder. The bitumen in a bituminous mixture can be described as the medium that envelops and bonds the mineral skeleton. In fact, it is not only the bitumen itself, but rather the mixture of bitumen and filler, i.e. the mastic, or the mixture of bitumen, filler and the fine aggregates, i.e. the mortar, that acts as a bridge between the coarser mineral aggregates.

The highest strains developing in an asphalt mixture appear in the mesoscale, the medium that connects the coarse mineral skeleton [1, 2]. Therefore it is particularly important to study and understand the durability at the mesoscale. Earlier studies have demonstrated that mastic [3] or mortar [4] should be considered as a more representative binding medium within the overall asphalt mixture. A crucial failure mechanism that asphalt pavements must endure, especially the base layer asphalt mixtures, is fatigue cracking. Two types of failure mechanisms can be expected between the mesoscale and the coarse mineral skeleton: adhesive failure, defined as loss of adhesion between stone and mortar phase, and cohesive failure, failure within the mortar phase.

Fatigue failure of asphalt mixtures is the result of repeated loading, where micro-cracks are initiated, propagating eventually into macro-cracks. In lab-scale, this phenomenon is simulated by various tests, such as flexural bending beam testing: 2- or 4-point Bending tests (2PB, 4PB), where a repeated loading of a specific strain or stress magnitude is applied until failure. The stages of a time-sweep test are distinguished in 3 phases. The first phase is characterised by a pronounced drop of stiffness modulus due to thixotropy and non-linearity (Phase 1), followed by a steady-almost linear- drop of stiffness (Phase 2). The end of the steady-state of stiffness drop signals the start of Phase 3 [5]. Similar fatigue mechanism has also been observed in bitumen [6-10], mastic [8, 10-14] and mortar [15-18]. Other studies have attempted to connect those scales, either by investigating straight correlations [7, 8, 12, 19] or by modelling the properties of different scales [20-22]. Other researchers expressed the interlinking of the scales by upscaling the meso-scale characteristics to the bulk asphalt-scale [15, 18, 23].

Many definitions of mortar can be found in literature, with the two main differences being the maximum aggregate size, varying from 0.5 mm to 2.36 mm, and the compaction method, namely self-compacted or aided. The

advantage of self-compacted mastic or mortar samples is the relatively small sample size and complex shapes that can be cast into. One discouraging point is that a certain level of viscosity is necessary to enable sufficient self-compaction of the sample, using either bitumen-rich samples or elevated mixing/fabrication temperatures. Naturally, self-compacted samples are limited to smaller max aggregate size, typically between 0.5 mm and 1 mm. On the other hand, compacted samples are either drilled out of compacted cylindrical tablets [24] or compacted in metal moulds [25]. Those samples are also known as Fine Aggregate Matrix (FAM). Since the self-compacted samples may contain 2-3 times higher bitumen content compared to FAM samples, this leads to less stiff samples suitable to be tested by Dynamic Shear Rheometer (DSR) devices. In contrast, most FAM samples are tested by Dynamic Mechanical Analyser (DMA) devices. Both can test column-like samples under oscillation with the latter being able to apply higher torque levels. DMA devices can also run tensile and bending tests, meaning that they are equipped with more powerful motors compared to DSR. For bituminous mortars a DSR device is still powerful enough, however the user should take care not to exceed the maximum allowed torque.

Martono et al. have pointed out the advantages in terms of repeatability when column geometries are being used compared to samples fitted between parallel-plate geometries in DSR [26]. While cylindrical column geometries are very common for mortar fatigue testing, issues with unpredictable failure points have been reported in the past [15]. As a way of circumventing this failure point randomness, this study addresses the cohesive fatigue resistance of bituminous mortar samples introducing a new sample geometry. Due to the complexity of the developed geometry, self-compacted samples were preferred.

The main goal of this geometry is to ensure improved repeatability of results and cohesive failure within an expected zone. The objectives of this study are first, to evaluate the applicability of the new geometry and secondly to evaluate the application of various failure criteria for the characterisation of fatigue resistance of bituminous mortars. To achieve these objectives, initially, a finite element (FE) approach is employed to simulate the developed strain and stresses during an oscillatory test. Then, the fabricated samples are further assessed in terms of their homogeneity and air voids presence using Computed Tomography (CT) scans. Finally, the new geometry is evaluated experimentally, where two control mortar mixtures types, using different base bituminous binders, are tested in terms of their fatigue resistance under various failure criteria using a DSR.

2. Geometry considerations

2.1.1. *Geometry*

To date, several studies have already been done to establish an improved geometry for the determination of fatigue performance in bituminous blends. Among these efforts, the utilisation of column- and hyperbolic-shaped geometry seemed to capture the fatigue behaviour of bituminous blends with sufficient repeatability [11, 15]. Initiated by the already performed geometric manipulations in parallel with the limitations that a DSR may have, a new geometry is proposed here. For the design of the new geometry, certain factors were taken into account, with the main motivation being to achieve fatigue cracking in a predefined zone of the specimen.

Contrary to previous studies, the effective height was divided into three equal parts. Thus, necking of the cylindrical specimen was preferred for the central part with a total height of 4 mm, whereas the two outer parts of equal height (4 mm) initiating from the rings, had a decreasing diameter. More specifically, the radius of the curved parts was selected in such a way to tangential approach the middle full cylindrical part. Concerning the height of the rings, this was chosen to be 4 mm to ensure proper adhesive strength with the mortar specimen and allow the specimen to be adequately clamped in the DSR.

The final selection of the diameter along the height of the specimen was based on two key criteria; for homogeneity issues, the minimum diameter of the sample was kept larger than three times the maximum diameter of the sand particle. Secondly, the two outer parts of the specimen should approach the middle section in such a way that the irregularities and geometry imperfections are minimised. It was found that a hybrid geometry which consists of three parts, namely two half-one sheeted hyperboloids both approaching the diameter of a cylindrical middle part, fulfilled all the previous criteria. The proposed geometry is illustrated in Figure 1.

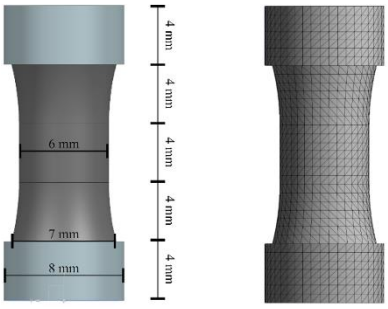

Figure 1: Schematic geometry of the mortar sample (left) and FE mesh (right).

2.1.2. *Finite Element implementation*

The new geometry was implemented in two Finite Element (FE) software packages, namely Siemens NX Nastran 11.0 and Ansys 2019 R3, for preliminary investigations [27, 28] to account for computational variations. After introducing the geometry in both software packages, the following material properties were provided as input: Poisson's ratio v = 0.4 and complex modulus G* = 200 MPa, based on the average complex modulus of the mortar at an intermediate temperature. The selection of the Poisson's ratio was based on the range of values (0.30-0.40) reported previously for asphalt mixtures [29, 30]. Following past efforts to model bituminous mortars [15], it is fairly certain that the Poisson's ratio should be slightly increased for the mortar mixture on fatigue testing compared to studies suggesting typical average values (0.35) for asphalt mixtures, due to the lack of coarse aggregates and the major presence of fines and bitumen in the mortar samples, resulting in a softer mixture. Concerning the value of the complex modulus, this was derived from preliminary fatigue tests in DSR at 17.5 °C (intermediate utilised temperature) with a frequency of 10 Hz.

A 3-D mesh of tetrahedrons was introduced in the whole geometry (Figure 1). Given the torque limitations of the DSR, the maximum torque T_{lim} (approximately 80 Nmm) was applied as torsional loading on the upper ring. Corresponding to the actual fatigue test in the DSR, the bottom ring was completely clamped.

During an actual shear test, the G* generated by the DSR (G^*_{raw}) is correct only for the case of perfect cylindrical samples, but not for the new geometry and hence needs to be corrected. Correction factors (CF) can be back-calculated to estimate the G^*_{real} values that correspond to the current geometry based on the Saint-Venant's torsional theory. An additional geometry of a perfect 6 mm cylinder was implemented for FE analysis. This consideration aimed to compensate between the new geometry and the given input of a perfect cylinder (6 mm) in DSR. Saint -Venant's torsion theory computes the theoretical value of complex modulus of a perfect cylinder based on the ratio of τ and γ in Eq.1, which can be further defined by Eq. 2 and 3.

$$G^* = \frac{\tau}{\gamma} \tag{1}$$

$$\tau = \frac{2T}{\pi R^3} \tag{2}$$

$$\gamma = \frac{\theta R}{h} \tag{3}$$

where τ is the shear stress, γ is the strain, T is the torque, R is the radius, θ is the deflection angle and h is the effective height.

Provided that for the new geometry the maximum shear stresses and strains occur in the middle part the following factors CF, CF_A and CF_B were introduced for shear stress and strain respectively, as expressed by Eq. 4 and 5.

$$\tau = a\frac{2T}{\pi R^3} = CF_A T \tag{4}$$

$$\gamma = \beta\frac{\theta R}{h} = CF_B \theta \tag{5}$$

The factors α and β allow for the estimation of the error between the actual and the pseudo-calculated stress, strain and subsequently complex modulus from the DSR and by assuming the R and h to remain somewhat similar can be eventually merged to the factors CF_A and CF_B. It is assumed that the G* of the new hybrid geometry will be within two extreme cases of hypothetical perfect cylindrical samples with a diameter of 6 and 7 mm. Therefore, a correction factor is required for the hybrid geometry, since the DSR will only estimate values correctly for geometry inputs of full/perfect cylinders. A simple hypothetical comparison of the theoretical between the perfect cylinders with 6 and 7 mm diameter, assuming the same T and θ, leads to a cumulative $CF_C = CF_A / CF_B = 0.5398$ for the two extremes according to the following calculations of Eq. 6.

$$\frac{G^*_{7\,mm}}{G^*_{6\,mm}} = \frac{\frac{\tau_{7\,mm}}{\gamma_{7\,mm}}}{\frac{\tau_{6\,mm}}{\gamma_{6\,mm}}} = \frac{R^4_{6\,mm}}{R^4_{7\,mm}} = 0.5398 \tag{6}$$

Thus, a comparison of the shear stresses and strains of a perfect cylindrical shape specimen with the currently introduced geometry for the worst-case scenario of the maximum torque will allow the back-calculation of the CF, which in this case should be within the range of $0.5398 < CF_C < 1$, based on the theoretical values.

Based on the design considerations discussed above, the FE results revealed that the highest shear stresses and strains appear in the middle cylindrical part for both FE implementations as depicted in Figure 2 and Figure 3. The highest maximum shear stresses and strains vary slightly between the two software packages. Next, the FE analysis of a perfect 6 mm cylinder was performed and revealed a maximum shear stress of 1.8892 MPa in the middle of the cylinder, which is almost in agreement with the theoretical value from Saint Venant's theory (τ_{6mm}) of 1.8862 MPa. The corresponding shear strain was calculated as 0.0094393 mm/mm. The geometry of 6 mm radius and 12 mm height, is inserted as specimen dimensions in the DSR software prior to testing.

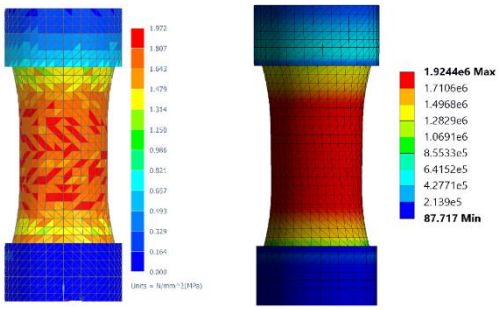

Figure 2: Maximum shear stresses of the new geometry calculated using the Siemens NX Nastran (left) and the Ansys 2019 R3 (right) software packages.

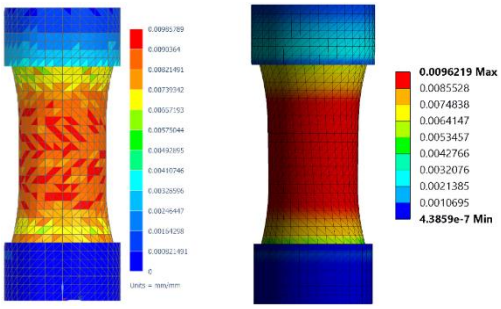

Figure 3: Maximum shear strains of the new geometry calculated using the Siemens NX Nastran (left) and the Ansys 2019 R3 (right) software packages.

To further clarify the corrections factors of the previous analyses, preliminary experimental tests proved that the failure occurs in the middle part. The CF for this part, where failure was imposed to be initiated, was calculated accordingly. The corrections factors were found to be, based on the different FE software and using Eq. 4 and 5, in the range of $1.0186 < CF_A < 1.0430$ and $1.0193 < CF_B < 1.0443$, for the shear stress and strain respectively. The ratio of these two correction factors implies the computation of the cumulative CF for the calculation of the G^*_{real}, namely $0.9988 < CF_C < 0.99930$. Average values of these factors were used, as failure was always observed in the middle cylindrical part.

3. Materials & sample preparation

3.1. Bituminous mortar materials and mix design

The bituminous mortar used in this research is based on the mix design of an asphalt concrete (AC) mixture. In this study, the fine skeleton used in the mortar is defined as the part of the mineral skeleton that is passing the 0.5 mm sieve. The gradation curves of the mortar and asphalt mixture are presented in Figure 4. Two commercial binders were considered to produce two mortar types. Binder A is an unmodified penetration grade bitumen, and binder B is an SBS polymer modified bitumen (PMB). Both were used to produce the bituminous mortars A and B, using the mix design presented in

Table 2. The conventional properties of A and B are presented in Table 1.

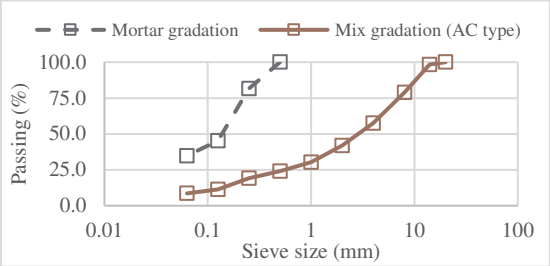

Figure 4: Asphalt mix gradation and corresponding mortar gradation curves.

Table 1: Conventional binder properties of A and B.

Bitumen type	Penetration (0.1 mm) EN 1426:2015	Softening point (°C) EN 1427:2015
A (35/50)	42.0	53.4
B (25/55-70)	40.0	74.2

The bitumen in an asphalt mixture covers both coarse and fine aggregates. Therefore to estimate the binder content of mortar, only the part of bituminous binder that covers the fine aggregates is taken into account out of the total. The Hveem-Edwards surface area is used to calculate the coverage. Details concerning the binder content calculations can be found elsewhere [16]. Originally, the calculated binder content represented 12.54 % of the total mortar mass mixture, as depicted in

Table 2. However, it was found that the mortar was not workable enough and as a consequence, not self-compacting, which is required to avoid air-voids.

When air is trapped in the bulk of the samples creating cavities, this will lead to weak spots and therefore to uncontrollable cracking. Therefore, the binder content was enriched to achieve the right workability. Preliminary work showed that by increasing the binder mass by a factor of 2.4, that would lead to a workable mortar mix. This factor is not strictly recommended for all mixtures types but depends on the binder content of the asphalt mixture and the desired workability. The original bitumen proportion multiplied by a factor of 2.4 led to a new value of 30.10 % (= 12.54 % × 2.4), which increases the total amount of the mix to 117.56 % (= 30.36 + 23.70 + 33.40 + 30.10). For this reason, all the fractions were adjusted again back to 100 %. For example, the bitumen content in the enriched formation is estimated as follows: (30.10 % / 117.56 %) = 25.61 %. The rest of the aggregate fractions were adjusted accordingly, following the previous example, and having in mind that the fractions should retain approximately the same ratios among them as in the original composition. For example, the ratio of limestone to riversand for the two compositions is: (30.66 % / 23.70 %) = 1.29 for the original, and (25.83 % / 20.16 %) = 1.28 for the enriched, which are very similar.

Table 2:Mortar composition.

Component	Original (%)	Enriched (%)
Limestone 0/2 (<0.5 mm)	30.66 %	25.83 %
Riversand 0/1 (<0.5 mm)	23.70 %	20.16 %
Filler (type V28/38)	33.40 %	28.41 %
Bitumen (type A or B*)	12.54 %	25.61 %
Total	100.00 %	100.00 %

Bitumen types are presented in Table 1.

The samples used in this study were produced based on the enriched composition, which is presented in

Table 2. As depicted in Figure 5, the preparation and addition of the binder are done “cold”. Handling bituminous binders this way is more practical and efficient than adding it “hot” since it allows to control the added amount better. Furthermore, the required amount per batch is approximately 6 gram, which is very small amount and allows for the binder to condition fast to the required mixing temperature when added into the preheated mixing chamber.

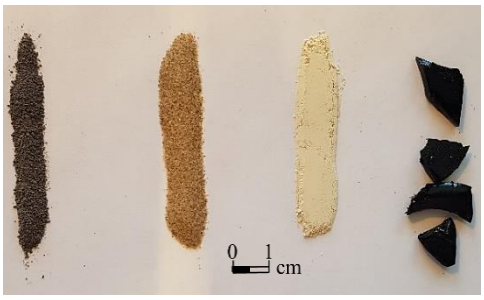

Figure 5: Mortar components (from left to right): limestone sand, river sand, filler and bitumen.

3.2. Sample fabrication

Since the mortar specimens are manufactured with a specific geometry, a casting mould that provides the correct shape is required. Silicone has been chosen as casting material since it has good heat resistance. Furthermore, silicone is stiff enough to hold the samples and flexible enough to release the samples easily. A spring-form with a diameter of 15 cm is used to cast the mould itself. Samples made by ABS (acrylonitrile butadiene styreneplastic) plastic were 3D-printed with identical geometry to provide the cavity of the desired shape. All materials and preparation of the casting mould are presented in Figure 6. An examples of fabricated sample together with its negative is exhibited in Figure 7.

The mortar components were mixed together using a Thermosel™ heating system (part of the Brookfield viscometer setup), to accurately control the mixing temperature, together with a mechanical mixer (see Figure 7). The mixing took place in two steps: first, the components were mixed for 5 min, and then the mould was filled for the first time. Afterwards, the rest of the mixture was mixed again for another 2 min, while the filled mould was stored in the oven at 180 °C, allowing the samples to release entrapped air voids. Finally, the rest of the mixed mortar material was added on top, filling possible loss of volume due to the de-airing action.

It was found that the capacity of a Brookfield chamber was ideal for preparing a set of 8 mortar samples (± 24 g). Besides, smaller amounts may lower the risk of heterogeneous samples. Temperatures in the range of 170 – 180 °C were reported in earlier studies as recommended fabrication temperature [31, 32]. However, for some samples of this study, it was proved insufficient to fully self-compact, showing visible cavities on the surface

of the samples. Subsequently, a small increase in temperature (+20 °C) was introduced to counteract this issue. To evaluate the effect of temperature, CT scans were utilised, as explained in 2.5. The final fabrication of the samples was made at 200 °C. One issue that may present here is the ageing level of the binder. It is likely that by using this fabrication method, a certain ageing level is induced to the binder. However, during lab-production of an asphalt mixture, it is expected that a comparable binder ageing will take place since the binder is exposed to high temperatures (180 °C) and even for a longer time compared to the mortar fabrication. Depending on the sample size, the binder is preheated from 30 min till 2.5 hours for asphalt mix production whereas for mortar fabrication the bitumen is added cold.

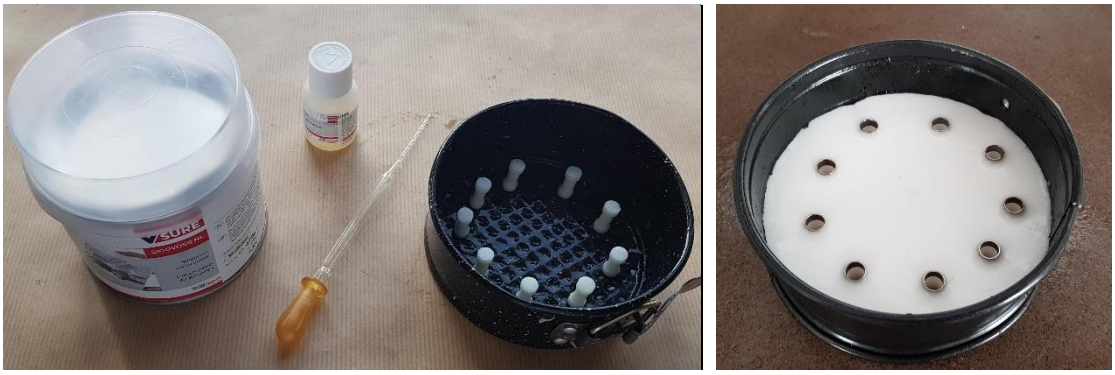

Figure 6: Preparation of casting mould: two-component casting silicone together with a spring-form and nine 3D-printed samples(left); ready-to-use casting silicone mould with steel rings (right).

Figure 7: Mixing setup: Thermosel heating system and mechanical mixer (left); fabricated mortar sample and 3D-printed sample (right).

4. Experimental investigation

4.1. Homogeneity and air voids

To assess the homogeneity level and the air voids of the mortar samples, Computed Tomography (CT) scans of bituminous mortar samples were performed. A high-resolution industrial CT scanner Phoenix X-ray nanotom system (TU Delft) was used to scan the mortar samples. Two mortar samples of mortar type A were scanned under

two different mixing temperatures; the first sample was mixed at 180 °C (sample A_{180}) and the second at 200 °C (sample A_{200}). The aim here was, first, to evaluate the effect of mixing temperature and, second, to assess the homogeneity of the mortar samples. The sample was attached (glued) on a glass rod to ensure a stable base during scanning. The sample was placed at a certain position away from the beam in order to achieve a full-frontal view of the sample between the rings. This positioning resulted in a voxel of 5 μm^3. The analysis and reconstruction of the CT scans were performed using the 3D image processing software Synopsys Simpleware ScanIP [33].

To obtain the volumetric composition of the samples, first, a median smoothing filter was applied to reduce noise and improve the quality of the CT scan images. Then a segmentation algorithm was applied, based on thresholds of greyscale pixel intensity, to distinguish the different material phases. Even though the mortar samples had five different phases, i.e. bitumen, filler, river sand, limestone sand, and voids, the resolution of the images did not allow for the segmentation of the filler phase. Hence, four phases were distinguished, namely the voids, the river sand, the limestone sand and the mastic, which included the filler and bitumen phases. After the segmentation process was completed, image analysis was performed to extract quantitative information on the microstructure of the samples.

4.2. Fatigue testing programme

The fatigue testing programme consists of two intervals: firstly, the sample is tested under low stress or strain oscillation (within the linear viscoelastic region) for 20 min in order to condition the sample at the desired temperature (thermal equilibrium interval). Secondly, the requested stress or strain is applied until the sample fails (time-sweep interval). In total, 46 mortar samples were tested under different temperatures and loading conditions (Table 3). The fatigue results are analysed based upon the failure criteria and approaches explained in section 2.6. For the SC tests, most tests were performed in increments of 0.15 MPa, starting from 0.95 MPa up to 1.40 MPa, including some stress levels in between. For the DC tests, the samples were subjected to strains ranging from 0.5% to 1.5%, in increments of 0.25%. The DC tests were limited, since the aim was not to build a robust full fatigue line but rather to provide indications concerning the effect of the loading condition on the dissipated energy approaches and on the mortar type.

Table 3: Overview of tested replicates per mortar type, loading mode and temperature.

Mortar type	Loading Mode	T (°C)	Number of replicates
A	SC	15.0	17
B	SC	15.0	11
A	DC	15.0	5
B	DC	15.0	5
A	SC	12.5/15.0/17.5/20.0	4*

B	SC	12.5/15.0/17.5/20.0	4*

* one replicate per type and per temperature

The most common approach to determine fatigue resistance of bituminous materials is by applying time-sweep tests under constant displacement or stress control until the gradual deterioration of the sample [7, 13, 34]. To investigate the fatigue resistance of bituminous mortars both stress-controlled (SC) and displacement-control (DC) time sweep tests were used in this study, performed at 10 Hz and 15 °C. DSR data were recorded every 1 sec (or every 10 cycles) for short tests and every 10 sec (or every 100 cycles) for more extended tests. The measurements were performed using an Anton Paar DSR (model MCR 102), equipped with a temperature-control chamber (type CTD 180) and the mortar samples were mounted using the Solid Circular Fixture (SCF) of the DSR (Figure 8). The tests were performed until the complete failure of the specimen. An event control was set for the termination of the test when the deflection angle exceeds 20°, which was proved high enough to observe complete fracture of the sample. An example of a broken sample after completion of the fatigue test is depicted in Figure 8.

Figure 8: DSR MCR 102 (left), sample mounted in the SCF holder (middle) and a damaged sample after test completion (right).

Various failure criteria and models have been employed to describe the fatigue failure of bituminous materials. In this study, the time-sweep results will be analysed based on four criteria. First, the empirical fatigue criterion N_{f50} [5], where failure is defined as the point at which G* reaches 50% of the initial value (G^*_{ini}). In order to account for thixotropic and non-linearity phenomena, G* of the 100th cycle is considered as G^*_{ini}. Second, the phenomenological approach of the "transition point", which defines as failure moment the maximum point when plotting the product of G* and cycles against cycles ($N_{f,G^*\times C}$) [35]. Both approaches can describe the fatigue resistance as a power function to a log-log plot of N_f (loading cycles to failure) as a function of applied stress (or strain), as described by Eq. 7 and 8.

$$N_{f,50} = A_{SC\_f,50}(\tau)^{B_{SC\_f,50}} \quad or \quad N_{f,50} = A_{DC\_f,50}(\varepsilon)^{B_{DC\_f,50}} \tag{7}$$

$$N_{f,G^*\times C} = A_{SC\_f,G^*\times C}(\tau)^{B_{SC\_f,G^*\times C}} \quad or \quad N_{f,G^*\times C} = A_{DC\_f,G^*\times C}(\varepsilon)^{B_{DC\_f,G^*\times C}} \tag{8}$$

where A and B are regression coefficients, during two loading conditions (SC or DC) and the two conventional failure criteria ($f, 50$ and $f, G^* \times C$) , τ is shear stress and ε is shear strain.

The third and fourth criteria are two energy approaches, namely the Dissipated Energy Ratio (DER) and the Ratio of Dissipated Energy Change (RDEC) [8, 36-38]. Due to the viscoelastic behaviour of bituminous materials, the dissipated energy (DE) per loading cycle can be calculated using Eq. 9. For the DER, the point when the DER deviates 20% from the initial non-damage linear stage (N_{p20}) is being considered as the fatigue failure indicator (Eq. 10) [39, 40]. The fatigue life, based on the N_{p20} criterion, is expressed in function of the initial DE (w_0) (Eq. 11) [37, 39]. The RDEC concept was introduced as an improved approach of DER, which takes into account only a part of the DE that drives the specimen to damage, unlikely to the DER that uses the total DE at every cycle. More information concerning the concept of RDEC can be found elsewhere [8, 36, 38]. Based on the RDEC approach, a fundamental energy parameter can be estimated that can be used to express the fatigue life of a bituminous material against N_f, instead of using the applied stress or strain. Based on the RDEC approach, a unique energy parameter can be derived, namely the plateau value (PV) [36, 38]. RDEC can be calculated using Eq. 12. After the RDEC is calculated, the PV can be defined. In this study, the PV was simply calculated as the average RDEC of the 10 last points before N_{f50}, a moment which falls within the plateau stage. It has been demonstrated that the PV exhibits excellent relationship against the N_{f50}, for both asphalt mixtures and binders, providing with a fatigue model independent of temperature effect, material properties and loading mode [8, 38]. To investigate whether this observation applies for this testing method, additional tests were performed at different temperatures, and a limited number of specimens were tested under DC.

$$w_i = \pi \sigma_i \varepsilon_i \sin(\delta_i) \tag{9}$$

$$DER = \frac{\sum_{i=1}^{n} w_i}{w_n} \tag{10}$$

$$N_{p20} = A_{DER}(w_0)^{B_{DER}} \tag{11}$$

$$RDEC_{SC\_b} = \frac{w_b - w_a}{w_a(b-a)} \quad or \quad RDEC_{DC\_b} = \frac{w_a - w_b}{w_a(b-a)} \tag{12}$$

where w is the dissipated energy, δ is phase angle, A_{DER} and B_{DER} are the regressions coefficients for the dissipated energy ratio (DER) approach, a and b are cycles with $b > a$, $RDEC$ is the ratio of dissipated energy change at cycle b, during a cycle period of b-a cycles, for SC tests ($RDEC_{SC\_b}$) or for DC tests ($RDEC_{DC\_b}$), w_a and w_b is the dissipated energy at cycle a and b, respectively.

5. Results and discussion

5.1. CT scanning analysis

The homogeneity of the samples and the effect of the mixing temperature on the air voids of the mortar samples were evaluated by utilising CT scanning. Two mortar A samples were scanned, A_{180} and A_{200}, with the main difference in fabrication temperature, 180 °C and 200 °C respectively. Preliminary scans showed the need for external support to envelope the sample because the x-ray radiation was causing a slow but significant, for the scans, deformation of the sample. To that end, a thin layer of epoxy glue was applied circumferentially on the sample. The presence of the glue, as well as the variable diameter, were two factors that made the analysis of the samples a challenging task.

The fractional composition of the two samples is presented in Figure 9 and Figure 10. The analysis was focussed on 10 mm height of the sample, instead of 12 mm-the actual effective height, because the images close to the rings were distorted.

The river sand phase is similar and quite stable, along with the sample height for both A_{180} and A_{200}. According to this, we can conclude that no sand segregation is observed and that the mortar samples are homogeneous. On the contrary, the limestone and mastic phase show a difference in concentrations between the two samples. The algorithm that detects the phases is based on the detection of greyscale value thresholds, where each greyscale range represent each phase. The filler included in the mastic phases is also of limestone origin, which means that

the limestone fraction and the filler fraction show similar greyscale value colour (same density). Therefore the algorithm may have detected overlapping areas for the two concentrations, hence leading to different limestone and mastic concentrations. Finally, the estimated voids for both samples are low and stable along with the height, with A_{200} demonstrating lower voids (0.02% instead of 0.81% for A_{180}), which can be attributed to the elevated temperature from 180 to 200 °C.

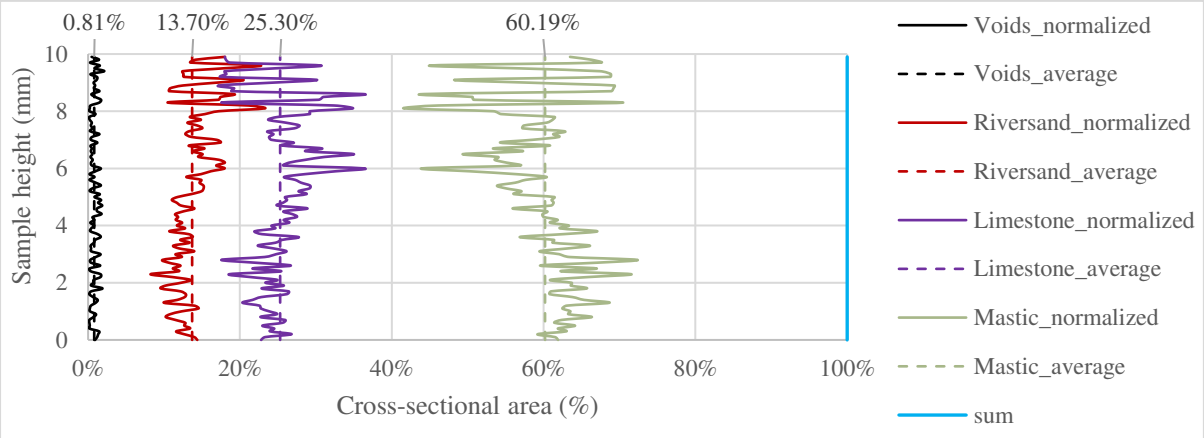

Figure 9: Composition of Sample A_{180} based on cross-sectional area distribution.

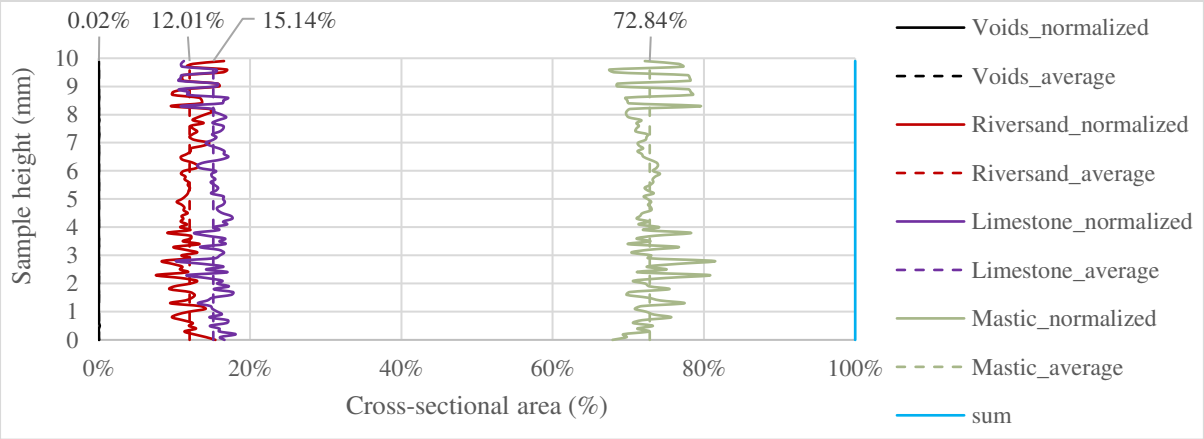

Figure 10: Composition of Sample A_{200} based on cross-sectional area distribution.

5.2. Fatigue testing analysis

5.2.1. *Empirical and phenomenological approach*

The fatigue lines are presented in Figure 11, 12, 13 and 14. The power fits presented in each figure are summarised in Table 4. For each power fit further details are presented, including details concerning the testing conditions, function parameters, the coefficient of determination (R^2) and at which figure these fatigue lines are presented.

Table 4: Summary of fatigue laws: testing conditions, fatigue law parameters and R^2.

Mortar type	Loading Mode	T (°C)	Fatigue law (power fit)	Intercept	Slope	R^2 (%)	Figure
A	SC	15.0	$N_{f,50}$ (τ)	13305.0	-7.07	93.6%	11
A	SC	15.0	$N_{f,G^* x C}$ (τ)	17377.0	-7.14	94.2%	
B	SC	15.0	$N_{f,50}$ (τ)	4523.0	-4.86	91.7%	
B	SC	15.0	$N_{f,G^* x C}$ (τ)	10887.0	-6.99	93.1%	
A	DC	15.0	$N_{f,50}$ (ε)	7333.7	-3.13	94.5%	12
A	DC	15.0	$N_{f,G^* x C}$ (ε)	7665.2	-3.23	98.8%	
B	DC	15.0	$N_{f,50}$ (ε)	10528.0	-4.79	94.0%	
B	DC	15.0	$N_{f,G^* x C}$ (ε)	15934.0	-4.99	93.4%	
A/B	SC	12.5/15.0/17.5/20.0	N_{p20} (w_0)	3325.8	-2.67	80.5%	13
A/B	DC	15.0	N_{p20} (w_0)	126370.0	-2.75	89.6%	
A/B	SC/DC	12.5/15.0/17.5/20.0	$N_{f,50}$ (PV)	4.3	-0.76	95.1%	14
A/B	SC/DC	12.5/15.0/17.5/20.0	$N_{f,G^* x C}$ (PV)	3.7	-0.81	93.4%	
A/B	SC/DC	12.5/15.0/17.5/20.0	N_{p20} (PV)	2.5	-0.83	97.8%	

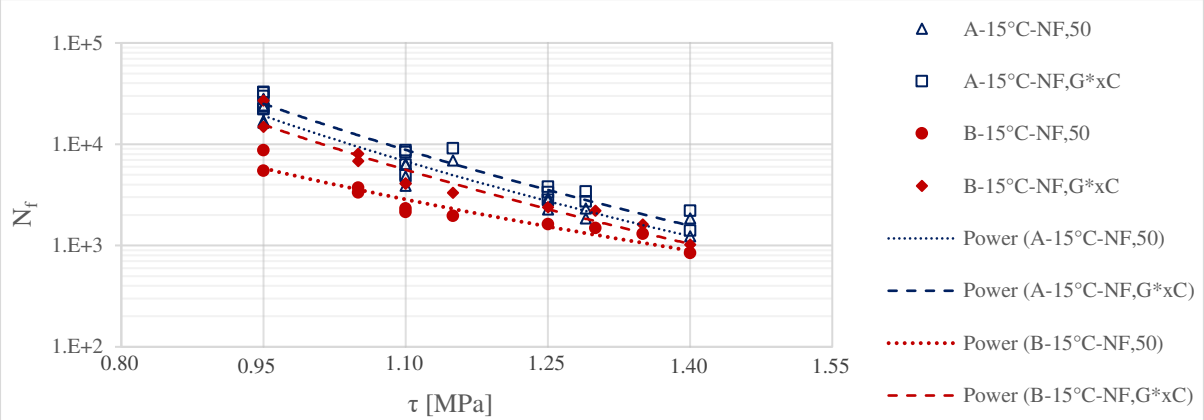

Figure 11: Fatigue resistance of mortar A and B in SC and 15 °C, based on failure criteria N_{f50} and N_{f,G^*xC}.

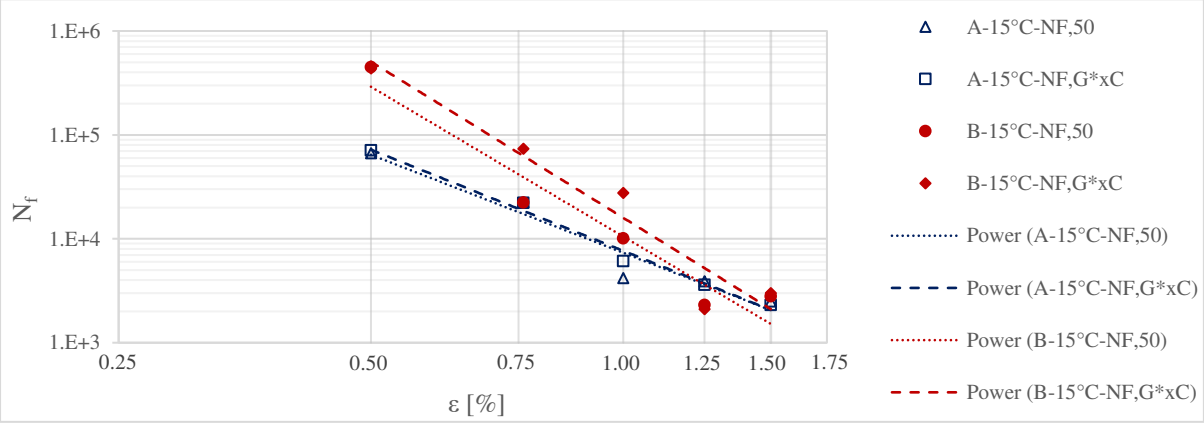

Figure 12: Fatigue resistance of mortar A and B in DC and 15 °C, based on failure criteria N_{f50} and N_{f,G^*xC}.

Comparing the two mortar types, A and B, it can be seen that the loading mode can have a significant impact on their fatigue life, as observed in Figure 11 and Figure 12. This is caused by the different binder type between the mortar types, with mortar A (unmodified binder-based mortar) indicating higher fatigue life in SC (Figure 11), while mortar B (SBS modified binder-based mortar) performed better in DC (Figure 12). In literature, it is reported that SBS-modified binders exhibit higher fatigue resistance compare to neat binders, due to the higher elasticity

introduced by the polymer, mainly based on strain-controlled tests, at binder [41] and mortar level [18]. However, studies using stress-controlled fatigue tests demonstrated similar fatigue resistance between neat and SBS-modified binders [42]. Overall, researchers agree that modified binders manifest different fatigue resistance behaviour which is dependent on the type of modification, base binder and chemical composition [43, 44]. It can be concluded here that when using empirical or phenomenological failure criteria, it is particularly important to consider the loading mode (SC or DC), depending on the type of binder. Overall, for the N_{f50} and N_{f,G^*xC}, both mortar samples for both loading modes (SC and DC) show a good fit with R^2 above 90%.

For mortar A, N_{f50} seems to be a good approximation for DC fatigue test since it almost matches the fatigue line of N_{f,G^*xC} (Figure 12). On the contrary, looking at the SC fatigue tests (Figure 11), there is a difference between N_{f50} and N_{f,G^*xC}. This observation is expected since the N_{f50} empirical failure criterion was initially developed for strain-controlled tests, and this can be confirmed here. For both SC and DC, the slopes are similar for N_{f50} and N_{f,G^*xC} (Table 4), which indicates that both failure criteria are independent of strain- or stress-level for the unmodified binder-based mortars. For mortar B, N_{f50} demonstrates lower fatigue resistance compared to N_{f,G^*xC}, for both SC and DC fatigue tests (Figure 11 and Figure 12). For DC tests, the slopes are similar for both N_{f50} and N_{f,G^*xC} , as also observed for mortar A, while for SC tests the fatigue lines of N_{f50} and N_{f,G^*xC} exhibit different slopes, showing stress-level dependency.

5.2.2. *Energy-based approaches: DER and RDEC*

Another approach to evaluate the fatigue resistance and to more comprehensively detect a transition in the damage level was introduced through the concepts of DER and RDEC. In this study, two loading modes, SC and DC, and various temperatures were introduced to evaluate the dependency of those parameters on the fatigue resistance of bituminous mortars, evaluated using DE concepts. Figure 13 shows the fatigue resistance of all samples in a log-log of N_{p20} versus w_0, based on the DER approach. According to the results, it is evident that fatigue resistance is independent of temperature and binder type but dependent on loading mode. Two fatigue lines are introduced with relatively high R^2, above 80% (Table 4), which consider the results of both mortar types tested at different temperatures but differentiating on the loading mode. The two fatigue lines have a similar slope but significantly different intercepts. It seems that for the same w_0, DC tests will lead to approximately 38× longer fatigue life compared to SC tests.

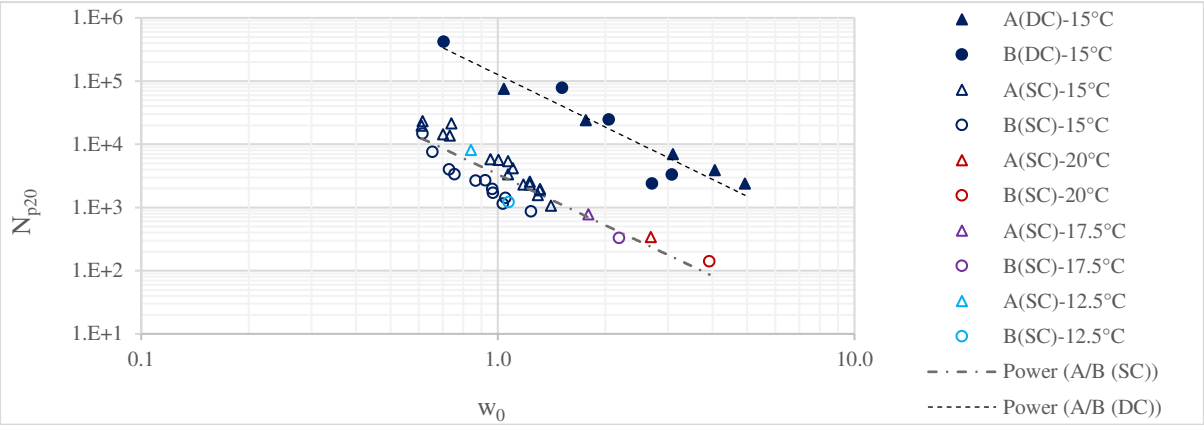

Figure 13: Fatigue resistance of mortar A and B in various loading modes and temperatures, according to the DER approach (N_{p20}).

Previous studies have demonstrated that PV relates very well against N_{f50}. This study will additionally examine the relationship of PV against N_{f,G^*xC} and N_{p20}. The fatigue lines are presented in Figure 14 and their power fit parameters in Table 4. For the set of conditions and data included in this study, it is possible to create fatigue lines using the PV, independent of testing conditions (temperature and loading mode) as well as material type. The data of mortar A tested in DC mode and 15 °C, deviate slightly from the fitted line, which is more noticeable for the N_{f,G^*xC} data. Overall, all three relationships exhibit very good fit, R^2>93%, with N_{p20} showing the best fit (97.8%). It is only reasonable that N_{p20} and PV exhibit an excellent relationship since both are based on the DE concept.

Additionally, most samples exhibited apparent damage and fracture signs in the middle area, as expected from the FE simulation. However, the samples tested at 17.5 °C and 20 °C, did not exhibit visible damage signs. These results might be attributed to flow phenomena or excessive creep instead of pure fatigue. Creep is expected to be a more realistic interpretation since the test was performed in SC mode, and no changes in the specimen geometry were observed after the test completion. However, since mortar samples can be tested at different loading modes or can have different stiffness, may show this transition between complete fracture due to fatigue to loss of modulus due to other phenomena (e.g. creep) at a different temperature from 15 °C. Therefore the PV value is recommended instead which, theoretically, represents a specific state of the material which can be achieved at different conditions for different materials. For the samples of this study, tests performed at a temperature above 15 °C showed a PV above 0.001. For that reason, the PV of 0.001 can serve as a threshold, which can be used as an indicative PV limit below that pure fatigue failure can be expected. On the other end, other studies have demonstrated the existence of the fatigue endurance limit, using the RDEC concept, above which the bituminous materials exhibit "*extremely long fatigue life",* as described by Shen and Carpenter [45], which is not examined in this study.

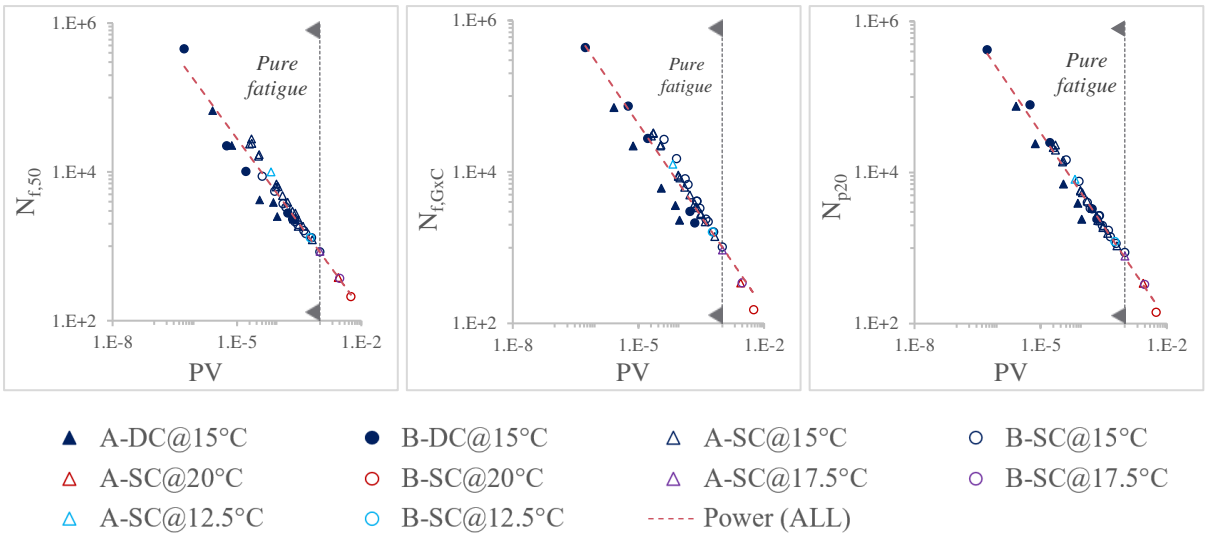

Figure 14: Fatigue resistance of mortar A and B in various loading modes and temperatures based on the RDEC approach: $N_{f,50}$ vs PV (left); $N_{f,G*\times C}$ vs PV (middle) and N_{p20} vs PV (right).

6. Conclusions and recommendations

In this paper, a new sample geometry is introduced, aiming to improve the fatigue resistance assessment of bituminous mortars. Additionally, to the theoretical design of the geometry and the practical fabrication steps, this study demonstrates the use of various failure criteria and concepts, and the challenges of using them to characterise the fatigue resistance. According to the results presented in this study, the following main conclusions can be drawn:

Sample integrity:

- The increase in mixing temperature from 180 to 200 °C has a positive effect on the elimination of air voids. Therefore, for the mortar types considered in this study, the mixing temperature of 200 °C is recommended to get reproducible samples.
- For samples of mortar A, no segregation of sand was observed and they were homogeneously mixed for both mixing temperatures (180 °C and 200 °C), as assessed by the CT scans.

Fatigue testing:

- The loading mode can have a significant impact when the N_{f50} and $N_{f,G*\times C}$ criteria are considered, especially in the case of SBS modified mortar. For SC tests, mortar A showed higher fatigue resistance while for DC tests mortar B performed better.

- It is particularly important to consider the loading mode (SC or DC) for fatigue tests, depending on the type of binder. Specifically, SC tests might underestimate the fatigue resistance of SBS PMB-based mortar types.
- The DC tests on mortar A showed similar fatigue resistance based on the N_{f50} and $N_{f,G^*\times C}$ failure criteria. Therefore, both criteria seem appropriate when evaluating neat binder-based mortars. On the other hand, mortar B exhibited different fatigue resistance for the two failure criteria, with N_{f50} showing lower fatigue resistance, which indicates that the N_{f50} is not a reliable fatigue failure indicator for SBS PMB-based mortar types.
- Both energy concepts, DER and RDEC, are material type and temperature independent. Only the RDEC proved to be also independent of the loading mode.
- Based on the PV, a unique fatigue line can be considered, which incorporates different materials (neat and modified mortar) tested under different conditions (loading mode and temperature).
- Very good relationship (R^2>93%) was demonstrated between PV and three failure criteria: N_{f50}, $N_{f,G^*\times C}$ and N_{p20}.
- A possible PV threshold (0.001) was observed based on the RDEC approach. Below this value failure is driven by pure fatigue and not by excessive creep. This can be used to check the suitability of the selected temperature and/or the applied loading for fatigue testing.
- When different materials are evaluated, energy concepts should be preferred instead of the N_{f50} and $N_{f,G^*\times C}$, with N_{p20} vs PV being the most consistent fatigue model.

Two commercial types of binders were considered in this study. Additional research could address the effect of different materials and additives, such as reclaimed asphalt binder and rejuvenators, using the proposed fatigue testing protocol. The CT scans were only considered for the unmodified binder, therefore the integrity of mortar type B was only considered indirectly based on the fatigue test results. Further investigations may be required to evaluate the effect of the mixing temperature on the air-voids of PMB mortars. Another critical aspect that can be studied by this testing method is the healing potential of bituminous mortars by incorporating rest periods. Finally, further investigation is necessary to evaluate the relationship between the fatigue properties on the meso-scale and the bulk-scale.

Acknowledgements

The first author would like to acknowledge the University of Antwerp for the PhD funding. Furthermore, Wim Verwaal and Ellen Meijvogel-de Koning from the Geoscience & Engineering Department at TU Delft are gratefully acknowledged for the CT scan analysis and NYNAS for providing the materials.

References

[1] T. Yi-qiu, Z. Lei, G. Meng, S. Li-yan, Investigation of the deformation properties of asphalt mixtures with DIC technique, Construction and Building Materials 37 (2012) 581-590.

[2] N. Hasheminejad, C. Vuye, A. Margaritis, B. Ribbens, G. Jacobs, J. Blom, W. Van den bergh, J. Dirckx, S. Vanlanduit, Investigation of Crack Propagation and Healing of Asphalt Concrete Using Digital Image Correlation, Applied Sciences 9(12) (2019) 2459.

[3] H. Wang, I.L. Al-Qadi, A.F. Faheem, H.U. Bahia, S.-H. Yang, G.H. Reinke, Effect of Mineral Filler Characteristics on Asphalt Mastic and Mixture Rutting Potential, Transportation Research Record 2208(1) (2011) 33-39.

[4] A. Margaritis, G. Tofani, G. Jacobs, J. Blom, S. Tavernier, C. Vuye, W. Van den Bergh, On the applicability of ATR-FTIR microscopy to evaluate the blending between neat bitumen and bituminous coating of reclaimed asphalt, Coatings 9(4) (2019).

[5] H. Di Benedetto, C. de La Roche, H. Baaj, A. Pronk, R. Lundström, Fatigue of bituminous mixtures, Materials and Structures 37(3) (2004) 202-216.

[6] C. Hintz, H. Bahia, Understanding mechanisms leading to asphalt binder fatigue in the dynamic shear rheometer, Road Materials and Pavement Design 14(sup2) (2013) 231-251.

[7] H. Soenen, C. de La Roche, P. Redelius, Fatigue Behaviour of Bituminous Materials: From Binders to Mixes, Road Materials and Pavement Design 4(1) (2003) 7-27.

[8] S. Shen, G.D. Airey, S.H. Carpenter, H. Huang, A Dissipated Energy Approach to Fatigue Evaluation, Road Materials and Pavement Design 7(1) (2006) 47-69.

[9] A.A.A. Molenaar, E.T. Hagos, M.F.C.v.d. Ven, Effects of Aging on the Mechanical Characteristics of Bituminous Binders in PAC, Journal of Materials in Civil Engineering 22(8) (2010) 779-787.

[10] B.S. Underwood, A continuum damage model for asphalt cement and asphalt mastic fatigue, International Journal of Fatigue 82 (2016) 387-401.

[11] M. Hospodka, B. Hofko, R. Blab, Introducing a new specimen shape to assess the fatigue performance of asphalt mastic by dynamic shear rheometer testing, Materials and Structures 51(2) (2018) 46.

[12] M.-C. Liao, J.-S. Chen, K.-W. Tsou, Fatigue Characteristics of Bitumen-Filler Mastics and Asphalt Mixtures, Journal of Materials in Civil Engineering 24(7) (2012) 916-923.

[13] G. Airey, M. Liao, N. Thom, Fatigue behaviour of bitumen-filler mastics, 10th International Conference on Asphalt Pavements - August 12 to 17, 2006, Quebec City, Canada, 2006.

[14] B. Xing, W. Fan, L. Han, C. Zhuang, C. Qian, X. Lv, Effects of filler particle size and ageing on the fatigue behaviour of bituminous mastics, Construction and Building Materials 230 (2020) 117052.

[15] L. Mo, M. Huurman, S. Wu, A.A.A. Molenaar, Research of Bituminous Mortar Fatigue Test Method Based on Dynamic Shear Rheometer, Journal of Testing and Evaluation 40(1) (2012) 84-90.

[16] W. Van den bergh, The effect of ageing on the fatigue and healing properties of bituminous mortars, Delft University of Technology, 2011.

[17] L. Mo, M. Huurman, S. Wu, A.A.A. Molenaar, Mortar fatigue model for meso-mechanistic mixture design of ravelling resistant porous asphalt concrete, Materials and Structures 47(6) (2014) 947-961.

[18] Y. Zhang, Z. Leng, Quantification of bituminous mortar ageing and its application in ravelling evaluation of porous asphalt wearing courses, Materials & Design 119 (2017) 1-11.

[19] C. Riccardi, A.J.d.B. Carrion, D.L. Presti, M. Losa, Reclaimed asphalt binders and mortars fatigue behaviour, Road Materials and Pavement Design 18(sup2) (2017) 281-292.

[20] J. Füssl, R. Lackner, Multiscale fatigue model for bituminous mixtures, International Journal of Fatigue 33(11) (2011) 1435-1450.

[21] B.S. Underwood, Y.R. Kim, Microstructural investigation of asphalt concrete for performing multiscale experimental studies, International Journal of Pavement Engineering 14(5) (2013) 498-516.

[22] C. Riccardi, A. Cannone Falchetto, M. Losa, M.P. Wistuba, Development of simple relationship between asphalt binder and mastic based on rheological tests, Road Materials and Pavement Design 19(1) (2018) 18-35.

[23] M. Huurman, L. Mo, M. Woldekidan, R. Khedoe, J. Moraal, Overview of the LOT meso mechanical research into porous asphalt raveling, Advanced Testing and Characterization of Bituminous Materials, Two Volume Set, CRC Press2009, pp. 523-534.

[24] P. Sousa, E. Kassem, E. Masad, D. Little, New design method of fine aggregates mixtures and automated method for analysis of dynamic mechanical characterization data, Construction and Building Materials 41 (2013) 216-223.

[25] S.R. Kommidi, Y.-R. Kim, L.R. de Rezende, Fatigue characterization of binder with aging in two length scales: sand asphalt mortar and parallel plate binder film, Construction and Building Materials 237 (2020) 117588.

[26] W. Martono, H.U. Bahia, J. D'Angelo, Effect of Testing Geometry on Measuring Fatigue of Asphalt Binders and Mastics, Journal of Materials in Civil Engineering 19(9) (2007) 746-752.

[27] Siemens Inc, Siemens Inc, NX Nastran 11, 2016.

[28] ANSYS Mechanical Application 2019 R3, ANSYS Mechanical Application 2019 R3,, 2019.

[29] T.-W. Hsu, K.-H. Tseng, Effect of Rest Periods on Fatigue Response of Asphalt Concrete Mixtures, Journal of Transportation Engineering 122(4) (1996) 316-322.

[30] A. Maher, T.A. Bennert, Evaluation of Poisson's Ratio for Use in the Mechanistic Empirical Pavement Design Guide (MEPDG), New Jersey Department of Transportation, 2008.

[31] W. Van den bergh, M.F.C. Van de Ven, The Influence of Ageing on the Fatigue and Healing Properties of Bituminous Mortars, Procedia - Social and Behavioral Sciences 53 (2012) 256-265.

[32] M. Woldekidan, M. Huurman, L. Mo, Nonlinear Response Characterization of Bituminous Mortar, Journal of Testing and Evaluation 40(5) (2012) 768-777.

[33] Synopsys Simpleware ScanIP, Synopsys Simpleware ScanIP, version Q-2019.12, 2019.

[34] C. Riccardi, A. Cannone Falchetto, M.P. Wistuba, M. Losa, Fatigue comparisons of mortars at different volume concentration of aggregate particles, International Journal of Fatigue 104 (2017) 416-421.

[35] G.M. Rowe, M.G. Bouldin, Improved techniques to evaluate the fatigue resistance of asphaltic mixtures, 2nd Eurasphalt & Eurobitume Congress Barcelona, 2000.

[36] K.A. Ghuzlan, S.H. Carpenter, Energy-Derived, Damage-Based Failure Criterion for Fatigue Testing, Transportation Research Record 1723(1) (2000) 141-149.

[37] A. Pronk, Evaluation of the Dissipated Energy Concept for the Interpretation of Fatigue Measurements in the Crack Initiation Phase Report No P–DWW–95–001, Road and Hydraulic Engineering Division of Rijkswaterstaat, The Netherlands (1995).

[38] S.H. Carpenter, S. Shen, Dissipated Energy Approach to Study Hot-Mix Asphalt Healing in Fatigue, Transportation Research Record 1970(1) (2006) 178-185.

[39] K.S. Bonnetti, K. Nam, H.U. Bahia, Measuring and Defining Fatigue Behavior of Asphalt Binders, Transportation Research Record 1810(1) (2002) 33-43.

[40] W. Van Dijk, Practical fatigue characterization of bituminous mixes, Journal of the Association of Asphalt Paving Technologists 44 (1975) 38-72.

[41] D.A. Anderson, Y.M. Le Hir, M.O. Marasteanu, J.-P. Planche, D. Martin, G. Gauthier, Evaluation of Fatigue Criteria for Asphalt Binders, Transportation Research Record 1766(1) (2001) 48-56.

[42] H. Liu, R. Luo, Development of failure criterion and fatigue model to characterize the fatigue resistance of asphalt binders under controlled-stress time sweep tests, Materials and Structures 53(1) (2019) 5.

[43] D.A. Anderson, D. Maurer, T. Ramirez, D.W. Christensen, M.O. Marasteanu, Y. Mehta, Field Performance of Modified Asphalt Binders Evaluated with Superpave Test Methods: I-80 Test Project, Transportation Research Record 1661(1) (1999) 60-68.

[44] J. Oliver, K.Y. Khoo, K. Waldron, The effect of SBS morphology on field prformance and test results, Road materials and pavement design 13(1) (2012) 104-127.

[45] S. Shen, S.H. Carpenter, Application of the Dissipated Energy Concept in Fatigue Endurance Limit Testing, Transportation Research Record 1929(1) (2005) 165-173.